Real-Time Polarimetry of Hyperpolarized ^{13}C Nuclear Spins using an Atomic Magnetometer

Kostas Mouloudakis,[†] Sven Bodenstedt,[†] Marc Azagra,[‡] Morgan W. Mitchell,[†] Irene Marco-Rius,[‡] and Michael C. D. Tayler[*,†]

[†]*ICFO – Institut de Ciències Fotòniques, The Barcelona Institute of Science and Technology, 08860 Castelldefels (Barcelona), Spain*

[‡]*IBEC – Institute for Bioengineering of Catalonia, 08028 Barcelona, Spain*

[¶]*ICREA – Institució Catalana de Recerca i Estudis Avançats, 08010 Barcelona, Spain*

E-mail: michael.tayler@icfo.eu

Abstract

We introduce a method for non-destructive quantification of nuclear spin polarization, of relevance to hyperpolarized spin tracers widely used in magnetic resonance from spectroscopy to in vivo imaging. In a bias field of around $30\,\mathrm{nT}$ we use a high-sensitivity miniaturized ^{87}Rb vapor magnetometer to measure the field generated by the sample, as it is driven by a windowed dynamical decoupling pulse sequence that both maximizes the nuclear spin lifetime and modulates the polarization for easy detection. We demonstrate the procedure applied to a $0.08\,\mathrm{M}$ hyperpolarized [1–^{13}C]-pyruvate solution produced by dissolution dynamic nuclear polarization, measuring polarization repeatedly during natural decay at Earth's field. Application to real-time quality monitoring of hyperpolarized substances is discussed.

TOC Graphic

dilute hyperpolarized ^{13}C spins

π_x π_y π_x π_y

nT

real-time magnetic field readout
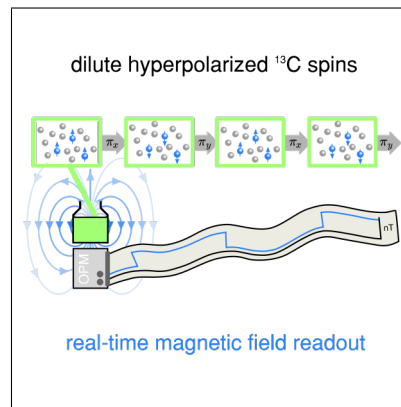
Keywords

Nuclear magnetism; Hyperpolarization; Optical Magnetometry; Polarimetry; Quantum control.

Magnetic resonance spectroscopy (NMR) and imaging (MRI) of nearly fully polarized (also known as "hyperpolarized") nuclear-spin ensembles is an emerging methodology[1–5] for probing cellular biochemistry in vitro, in vivo[6–9] and in perfused organs.[10] The magnetic moment of a hyperpolarized substance, which is proportional to the nuclear polarization, can be three to four orders of magnitude larger than that of thermally polarized substances,[11] resulting in MRI pixels that contain chemically specific signals high above the noise floor even at low concentration. In pre-clinical[12] and clinical[13,14] monitoring of metabolic diseases, hyperpolarized small molecules such as pyruvic acid are typically injected into a biosystem where metabolism takes place. Dynamic MRI of the downstream metabolites then provides biodistribution maps and kinetic rates to distinguish between healthy and diseased tissue.

In these and other applications, such as noble-gas MRI, there are several motives to quantify nuclear spin hyperpolarization. The magnitude of polarization, P (a dimensionless number ranging from 0, for unpolarized spins, to ± 1, when spins are completely polarized), determines the effective concentration of the substrate seen by MRI and therefore is a crucial parameter in kinetic models of spin-label transfer along a metabolic pathway, especially in cases where hyperpolarized agents are administered to the subject repeatedly.[15] Additionally, any exogenous substance introduced in vivo is subject to strict quality control and dose requirements. Given that many hyperpolarization technologies are at an early development stage and not always consistent, P is currently a control variable; for instance, in dissolution dynamic nuclear polarization, polarization is monitored both before[16,17] and after[18,19] sample dissolution. A reliable measurement of P may also provide a cost-per-unit signal enhancement metric to compare different hyperpolarization methods, which may be influential in future large-scale clinical or other applicability of hyperpolarized magnetic resonance.

A standard polarimetry method is *ex post* comparison of the hyperpolarized-NMR signal amplitude against the NMR signal of the same system after polarization has decayed back to a thermal equilibrium value.[18,19] This approach can be performed on a variety of NMR spectrometer systems in background fields from mT to T, but is slow and requires several

calibrations such as tuning of radiofrequency coils, pulse flip angles, and magnetic field; conventionally, although lower-field instrumentation may be less expensive, calibrations become much lengthier due to reduced-efficiency inductive pickup of the spin precession signals.[20] In special molecules one can also determine polarization from intensity patterns in spin-coupling multiplets, namely where the hyperpolarized substrate contains a second, ancillary spin label to be used as a "spy" nucleus, e.g., $[1,2\text{-}^{13}C_2]$-pyruvate[21–23] or $[2\text{-}^{13}C]$-acetate.[16] A third method is through detection of the bulk magnetic field, $\mathbf{B}$, produced by the hyperpolarized spins. For an ensemble of uncoupled spin-1/2 nuclei,

$$|\mathbf{B}| = \hbar\mu_0 PC\gamma k\,, \tag{1}$$

assuming that $\mathbf{B}$ is parallel to the polarization vector, where $\hbar$ is the reduced Planck constant, μ_0 is the vacuum permeability, C is the number density of spins, γ is the gyromagnetic ratio and k is a constant of proportionality that depends on the geometry of the sample and the position where $\mathbf{B}$ is measured. In the case of a uniformly polarized spherical sample of radius R, $k = (R/r)^3/3$ for position $r > R$ along the $\mathbf{B}$ direction.

Most bulk-protonated liquids have $|\mathbf{B}|$ on the order of pT to nT for $R/r \approx 1$, at thermal equilibrium in moderate fields, e.g., 1 T. A dilute hyperpolarized liquid ($PC \approx P_{\text{thermal}}C_{\text{bulk}}$) could produce fields of comparable magnitude, while a hyperpolarized neat liquid ($C \approx C_{\text{bulk}}$, $P \gg P_{\text{thermal}}$) will produce a considerably stronger field. One way to measure $|\mathbf{B}|$ is through Zeeman frequency shifts of a second, thermally polarized spin species in the liquid.[24] This, in addition to the above methods, however, relies on high-resolution NMR instrumentation (with which comes high cost and limited mobility) and the destruction of a significant part if not all of the hyperpolarized spin order. In the following, as an alternative, we demonstrate a direct, nondestructive measurement of $|\mathbf{B}|$ using an optically pumped magnetometer (OPM).[25–27] To obtain P, the factor k in Equation 1 is eliminated

using a reference sample of known polarization (P_{ref}) and concentration (C_{ref}):

$$P = \left(\frac{\gamma_{ref}}{\gamma}\right)\left(\frac{C_{ref}}{C}\right)\frac{|\mathbf{B}|}{|\mathbf{B}_{ref}|}P_{ref}. \tag{2}$$

Here the reference sample is ^{1}H spins in thermally polarized non-degassed milli-Q water at 2 T (^{1}H$_2$O; $C_{ref} = 110$ M, $P_{ref} \approx 6.8 \times 10^{-6}$).

A suitable pulse sequence to detect $\mathbf{B}$, assumed parallel to the z axis, is shown in Figure 1. Uniformly spaced π spin flips toggle the sign of the z component, producing a square wave that is distinct from background fields.[28] Flips are applied as π rotations alternately about x and y laboratory-frame axes making an XY4 cycle with repeating element ($\tau/2 - \pi_X - \tau - \pi_Y - \tau - \pi_X - \tau - \pi_Y - \tau/2$). The useful feature of XY4 is the dynamical decoupling of the background field from the spin system at the first-order average Hamiltonian level,[29] which allows us to neglect bias fields with strengths $|\mathbf{B}_{bias}| \ll 2\pi/\gamma\tau$.
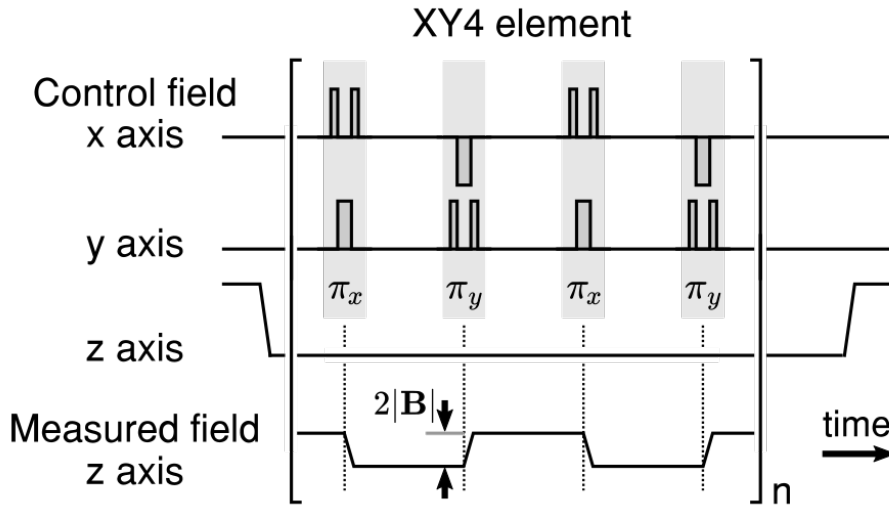
Figure 1: Experimental sequence. Upon field switching to near-zero fields, alternating $(\pi)_x \equiv (\pi/2)_x(\pi)_y(\pi/2)_x$ and $(\pi)_y \equiv (\pi/2)_y(\pi)_{-x}(\pi/2)_y$ dc pulses (making the XY4 cycle) periodically invert the nuclear magnetization. A magnetometer measures the z field component throughout.

The top panel of Figure 2 shows the NMR signal recorded during XY4 ($\tau = 50$ ms, 0.2 ms π-pulse length) for a 1 cm^3 cylindrical volume of 2-T-prepolarized water, using an alkali-
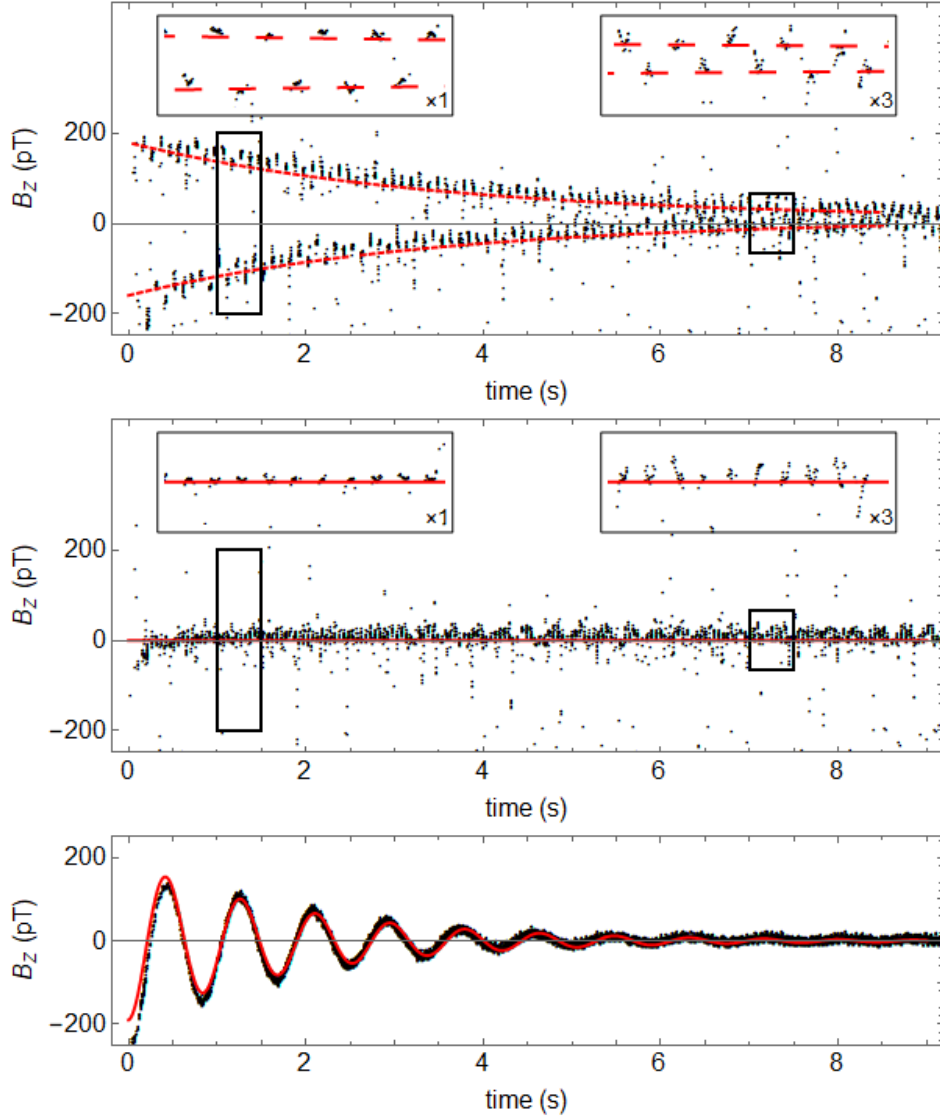
Figure 2: Measured z-axis component of magnetic field (B_z, relative to background) during the ultralow-field portion of the sequence shown in Figure 1. Single-shot signals are measured for $1\,\mathrm{cm}^3$ of H_2O using a ^{87}Rb-vapor OPM under the following conditions: (top) XY4 decoupling, sample prepolarized at $2\,\mathrm{T}$, (middle) XY4 decoupling, prepolarized at Earth's field, (bottom) free precession, i.e., without XY4 pulses, prepolarized at $2\,\mathrm{T}$. The red curves indicate fitting to square- or sine-modulated monoexponential decay curves with the time constants (top) $T_1 = 3.5\,\mathrm{s}$ and (bottom) $T_2^* = 2.0\,\mathrm{s}$.

6

metal-vapor OPM inside a magnetic shield (MS-1LF, Twinleaf LLC). The OPM measures the z-axis component, B_z, of total field using quadrature demodulation of the Hanle absorption resonance in a ^{87}Rb vapor.[30] The vapor is confined to a microelectromechanical system (MEMS) cell of approximate dimensions 4 mm $\times$ 4 mm $\times$ 1.5 mm at a standoff distance of 3 mm from the sample chamber. The magnetic shield provides a simple and convenient way to isolate the detector from unknown and/or time-dependent background magnetic fields. The shield presents no additional operating constraints; indeed, it allows the apparatus to be carried freely around the room, and placed within a few meters of an MRI scanner in background fields of several tens of mT without any need to compensate for background drifts. For further technical details of the OPM we refer the reader to the Supporting Information, plus past work.[31] The signal shown is processed minimally, where data points during each π pulse and up to 5 ms afterwards are excluded (where the magnetometer output saturates) and mains-hum noise is suppressed by applying a 45-to-55-Hz band-stop filter. The solid red curve: $B_z(t) = (190 \text{ pT}) \times \text{sgn}(\sin 20\pi t) \exp(-t/T_1)$ fits to the remaining data points. The decay time constant, $T_1 = 3.5$ s, is that of longitudinal relaxation under dynamical decoupling in the effective zero field, inclusive of the contribution due to imperfections in the π pulses.

The middle panel of Figure 2 shows the OPM signal when the starting magnetic field is much lower, $50\,\mu\text{T}$ or around Earth's field, where there is no major alternation seen above the noise background. As a comparison, the lower panel of Figure 2 shows the signal for 2-T-prepolarized water in the absence of XY4 decoupling. Here the free-decay signal is an exponentially decaying cosine wave $B_z(t) = (190 \text{ pT}) \times \cos(2.48\pi t) \exp(-t/T_2^*)$ with $T_2^* = 2.0\,\text{s}$, corresponding to precession in the approximately $30\,\text{nT}$ remanent field of the magnetic shield. The precession signal undergoes faster decoherence ($T_2^* < T_1$) due to gradients in the precession field, which are otherwise decoupled under XY4.

To apply XY4 to a system of hyperpolarized ^{13}C spins, the duration of each dc pulse is increased by a factor $\gamma_\text{H}/\gamma_\text{C} \approx 3.97$ to produce rotation angles of π and $\sim 4\pi$ on ^{13}C
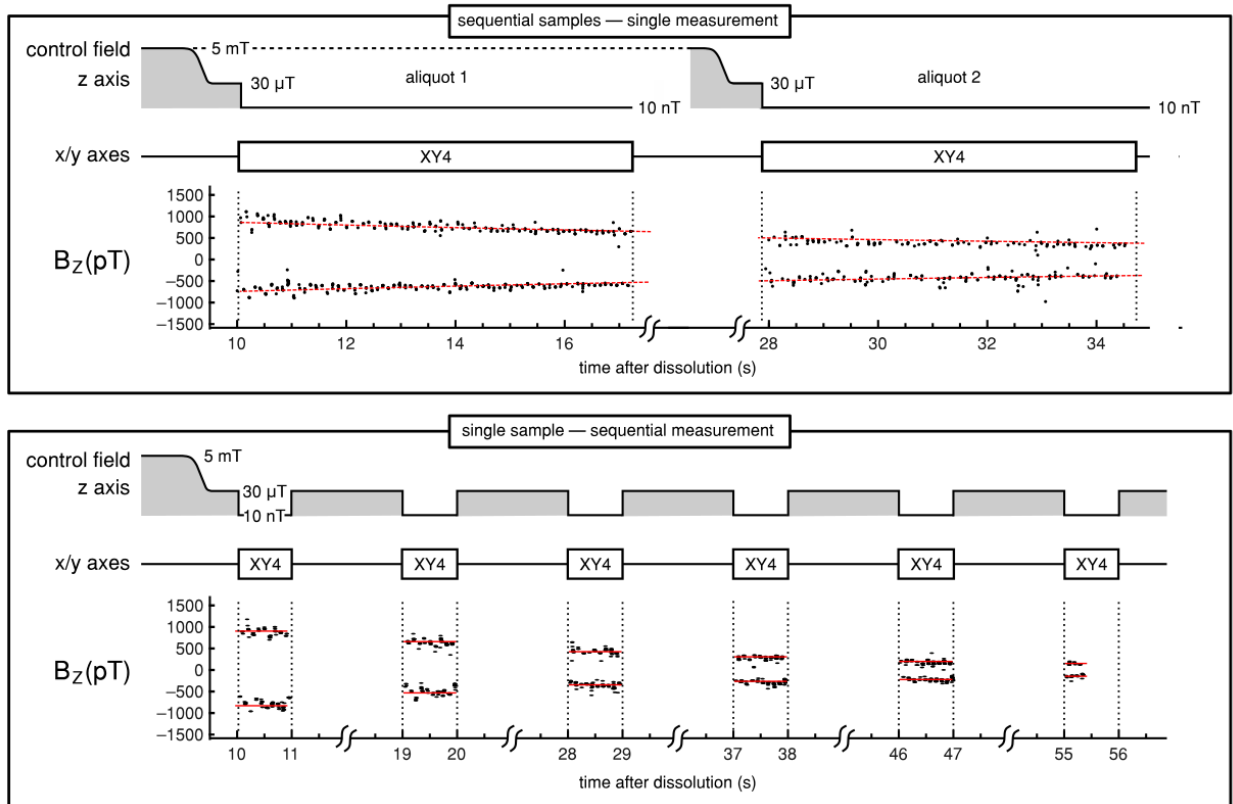
Figure 3: The NMR signals recorded for $0.08\,\mathrm{M}$ hyperpolarized [1-^{13}C]-pyruvate under ^{13}C XY4, $\tau = 50$ ms. Upper panel B_z data are obtained after portioning the hyperpolarized solution into two $1.0\,\mathrm{cm}^3$ aliquots, each stored at 5 mT and then placed sequentially next to the zero-field OPM. Red curves show monoexponential decays with fitted decay time constant $T_1(\mathrm{zero\,field}) = 24(1)\,\mathrm{s}$. The lower panel data were obtained with a single aliquot, by alternating 1-s acquisition periods at zero field with 8-s storage periods at $30\,\mu\mathrm{T}$. Signal loss in between acquisition periods is attributed to natural decay, fitted by the red curve to $T_1(30\,\mu\mathrm{T}) = 24(1)\,\mathrm{s}$, which within error is equal to $T_1(\mathrm{zero\,field})$.

and ^{1}H, respectively. In addition to dynamically decoupling small residual magnetic fields, this combination of angles also decouples the ^{13}C-^{1}H scalar (J_{CH}) coupling interaction when performed sufficiently quickly; $\tau \ll |1/J_{CH}|$. The polarimetry technique can therefore be applied across a wide range of organic molecules.

To demonstrate application to substances of clinical and pre-clinical relevance, we measured the OPM signal during ^{13}C XY4 dynamical decoupling for solutions of hyperpolarized [1-^{13}C]-pyruvic acid (PA = ^{12}CH$_3$^{12}CO^{13}COOH; $^3J_{CH}$ = 1.3 Hz). The samples were prepared initially as $24\,\mu L$ volumes of 0.2 wt.% OX-063 radical (GE Healthcare) and 0.09 wt.% Dotarem (Guerbet S.A., France) dissolved in neat-liquid PA (Sigma Aldrich). Each of these were polarized at $1.4\,K$ in a magnetic field of $3.5\,T$, using a commercial dissolution-DNP polarizer (HyperSense, Oxford Instruments Ltd.) via 40 minutes of positive-lobe microwave irradiation near 95 GHz. After polarization, the cryogenic samples were dissolved in a superheated phosphate-buffered-saline solution (4.5 cm^3 in ^{1}H$_2$O, 10 mM Na$_2$HPO$_4$, 2 mM KH$_2$PO$_4$, 1 wt.% HEPES, 0.01 wt.% EDTA, 0.1 wt.% NaCl, 0.2 wt.% NaOH) and ejected from the instrument at a temperature of $37\,°C$ into a vial, at a final concentration of $C = 0.080(1)$ M.

Immediately after the dissolution process, two 1.0 cm^3 aliquots of the polarized ^{13}C sample were collected and stored in the approximately 5 mT fringe magnetic field of the DNP polarizer. The procedure simulates a situation where fractions of a hyperpolarized sample are inserted into an MRI scanner one after the other.[15] The aliquots were then transferred sequentially by syringe into the magnetic shield located approximately 1 m from the polarizer and containing the OPM and sample chamber used for the 2-T-prepolarized water sample. A solenoid coil provided a guiding magnetic field[25] of $30\,\mu T$ over the syringe during transport. For the first aliquot, the guiding field was switched off around 10 seconds after dissolution and the XY4 sequence ($\tau = 50$ ms) was initiated and sustained for a time of 6-7 seconds. The liquid was then removed from the apparatus by syringe, the guiding field was switched on again, and the process repeated for the second aliquot; see Figure 3, upper

panel. During the time at zero field, the OPM signal was recorded, also shown in the upper panel of Figure 3. Signals were fit by a monoexponential decay envelope with time constant $T_1 = 24(1)$ s. The time constant is remarkably long, considering that the paramagnetic Dotarem (Gd^{3+}) and OX-063 species were not removed from the solution. This indicates a low seriousness of paramagnetism-induced relaxation in the zero-to-ultralow-field regime.[32] One explanation could be that although Gd^{3+} ions remains in the liquid after dissolution, their contact with ^{13}C spins is minimized due to chelation in the buffered solution. The initial amplitude of the ^{13}C signal, furthermore, is used to provide a lower-bound value for the polarization. Amplitudes of the signals for the first and second pyruvate aliquots, 1020 pT and 600 pT respectively, at zero decoupling time equate via Equation 2 to ^{13}C polarizations of $P = 12(1)$ % and 7(1) %, using the 190 pT reference signal amplitude for the 2-T-prepolarized water sample (Figure 2) and the other parameters as given above. The first one is in agreement with the *ex post* value $P = 13\%$ calculated from the hyperpolarized vs. thermal ^{13}C-NMR spectra of a third 1.0 cm^3 aliquot from the same batch, which was also injected at 10.0 s into a bench-top 1.5 T NMR spectrometer (Pulsar, Oxford Instruments Ltd.).

Sample polarimetry is not limited to one-off measurement. As the lower part of Figure 3 shows, hyperpolarized spins may be sustained across multiple zero-field measurements performed sequentially. After sample injection into the magnetic shield, the field is repeatedly and rapidly (<10 µs) toggled between the effective-zero field and a 30 µT holding field to emulate polarization storage in ambient magnetic field. In the case shown, 8-s storage intervals occur between 1-s zero-field observation windows. For $[^{13}C]$-pyruvate, signal decay occurring between windows can be fit to the monoexponential time constant $T_1 = 24$ s, which within error is the same as at zero field under XY4 decoupling. The observation that the ^{13}C T_1 is unchanged across three orders of magnitude in field is not so surprising for such a small molecule, given that paramagnetic relaxivities in aqueous solution are generally found to be constant below 1 mT.[32] We expect that the use of nonpersistent-radical polar-

izing agents,[33–36] filtration[37] or other strategies to remove paramagnetic dopants from the solution should prolong the decay time at both the storage and detection fields.

Given the growing interest in hyperpolarized MRI, a wide scope of application for the method is envisioned. Solid hyperpolarized [^{13}C]-pyruvate can be transported far away from where it is produced,[38,39] for instance to an MRI facility at a hospital located hundreds of kilometers away from the polarizer.[40] Nondestructive polarization measurement at the use end using a combined dissolution-and-magnetometry device may form part of the quality control procedure carried out upon liquification. Unlike conventional NMR, our technique does not rely upon maintaining a homogeneous magnetic field around the sample; this means that mandatory procedures for human in-vivo application including sample concentration—via absorption spectroscopy—and pH checks, could be measured in parallel. This may significantly reduce the delivery time into a human body, which currently stands around 1 minute after dissolution and incurs a substantial natural decay of the polarization.[19] Hyperpolarization procedures involving chemical reactions of parahydrogen at μT fields[41,42] should also be compatible with detection via OPMs, enabling real-time in-situ monitoring (or optimization) of polarization buildup.

Most liquid-state hyperpolarized NMR and MRI procedures focus on the study of specific chemical sites in isotopically pure compounds (for instance, the terminal carboxyl carbon in pure [1-^{13}C]-PA). However, it is possible, although uncommon, to hyperpolarize and study more than one isotopomer or compound at the same time, e.g., a solution of [1-^{13}C]-pyruvate and [1-^{13}C]-butyrate[43] or [^{13}C]-urea.[44] The present version of our experiment does not allow polarimetry of two alike spin species at the same time and therefore the magnetometry procedure would have to be performed on the component pure solutions before mixing. In principle, isotopomer-selective π pulses that exploit the chemically specific Zeeman shifts and/or spin-spin J couplings could be used to achieve selectivity in mixtures. Various other schemes may also be possible, such as magnetic gradiometry of two chemically identical samples that have opposite polarization in one of the compounds.

As a final remark, the square-wave NMR signal may in principle be recorded at any magnetic field, given a sufficiently sensitive detector. In this work, the nT bias field was chosen to use a zero-field OPM of sensitivity around $10\,\mathrm{fT}/\sqrt{\mathrm{Hz}}$,[31] although the technical noise background (such as mains hum noise) is much larger, on the order of $1\,\mathrm{pT}/\sqrt{\mathrm{Hz}}$. Miniaturized versions of zero-field OPMs are produced on a medium commercial scale[45,46] for research use in magnetoencephalography[47,48] and other biomagnetic imaging studies. While these must operate in shielded environments for highest performance,[49,50] other types of OPMs and magnetic gradiometers can reach sensitivities of tens of $\mathrm{fT}/\sqrt{\mathrm{Hz}}$ at ambient field[51] while also being less susceptible to background noise. In the future, these may remove the current experimental requirement of a magnetic shield.

Acknowledgement

Supporting Information Available

Additional experimental details including photographs of the experimental setup (PDF).

References

(1) Aquaro, G. D.; Menichetti, L. Hyperpolarized ^{13}C-Magnetic Resonance Spectroscopy. *Circulation: Cardiovascular Imaging* **2014**, *7*, 854–856.

(2) Comment, A.; Merritt, M. E. Hyperpolarized Magnetic Resonance as a Sensitive Detector of Metabolic Function. *Biochemistry* **2014**, *53*, 7333–7357.

(3) Brindle, K. M. Imaging Metabolism with Hyperpolarized ^{13}C-Labeled Cell Substrates. *Journal of the American Chemical Society* **2015**, *137*, 6418–6427.

(4) Wang, Z. J.; Ohliger, M. A.; Larson, P. E. Z.; Gordon, J. W.; Bok, R. A.; Slater, J.; Villanueva-Meyer, J. E.; Hess, C. P.; Kurhanewicz, J.; Vigneron, D. B. Hyperpolarized ^{13}C MRI: State of the Art and Future Directions. *Radiology* **2019**, *291*, 273–284.

(5) Jørgensen, S.; Bøgh, N.; Hansen, E.; Væggemose, M.; Wiggers, H.; Laustsen, C. Hyperpolarized MRI – An Update and Future Perspectives. *Seminars in Nuclear Medicine* **2022**, *52*, 374–381.

(6) Marco-Rius, I.; Comment, A. In vivo hyperpolarized ^{13}C MRS and MRI applications. *eMagRes* **2018**,

(7) Marco-Rius, I.; Wright, A. J.; en Hu, D.; Savic, D.; Miller, J. J.; Timm, K. N.; Tyler, D.; Brindle, K. M.; Comment, A. Probing hepatic metabolism of [2-^{13}C]dihydroxyacetone

in vivo with ^{1}H-decoupled hyperpolarized ^{13}C-MR. *Magnetic Resonance Materials in Physics, Biology and Medicine* **2020**, *34*, 49–56.

(8) von Morze, C.; Tropp, J.; Chen, A. P.; Marco-Rius, I.; Criekinge, M. V.; Skloss, T. W.; Mammoli, D.; Kurhanewicz, J.; Vigneron, D. B.; Ohliger, M. A. et al. Sensitivity enhancement for detection of hyperpolarized ^{13}C MRI probes with ^{1}H spin coupling introduced by enzymatic transformation in vivo. *Magnetic Resonance in Medicine* **2017**, *80*, 36–41.

(9) Can, E.; Bastiaansen, J. A. M.; Couturier, D.-L.; Gruetter, R.; Yoshihara, H. A. I.; Comment, A. [^{13}C]bicarbonate labelled from hyperpolarized [1-^{13}C]pyruvate is an in vivo marker of hepatic gluconeogenesis in fasted state. *Communications Biology* **2022**, *5*, 10.

(10) Merritt, M. E.; Harrison, C.; Storey, C.; Jeffrey, F. M.; Sherry, A. D.; Malloy, C. R. Hyperpolarized ^{13}C allows a direct measure of flux through a single enzyme-catalyzed step by NMR. *Proceedings of the National Academy of Sciences* **2007**, *104*, 19773–19777.

(11) Ardenkjær-Larsen, J. H.; Fridlund, B.; Gram, A.; Hansson, G.; Hansson, L.; Lerche, M. H.; Servin, R.; Thaning, M.; Golman, K. Increase in signal-to-noise ratio of >10,000 times in liquid-state NMR. *Proceedings of the National Academy of Sciences* **2003**, *100*, 10158–10163.

(12) Ros, S.; Wright, A. J.; Bruna, A.; Caldas, C.; Brindle, K. M. Metabolic imaging with hyperpolarized [1-^{13}C] pyruvate in patient-derived preclinical mouse models of breast cancer. *STAR Protocols* **2021**, *2*, 100608.

(13) Gallagher, F. A.; Woitek, R.; McLean, M. A.; Gill, A. B.; Garcia, R. M.; Provenzano, E.; Riemer, F.; Kaggie, J.; Chhabra, A.; Ursprung, S. et al. Imaging breast cancer using

hyperpolarized carbon-13 MRI. *Proceedings of the National Academy of Sciences* **2020**, *117*, 2092–2098.

(14) Woitek, R.; Gallagher, F. A. The use of hyperpolarised ^{13}C-MRI in clinical body imaging to probe cancer metabolism. *British Journal of Cancer* **2021**, *124*, 1187–1198.

(15) Lees, H.; Millan, M.; Ahamed, F.; Eskandari, R.; Granlund, K. L.; Jeong, S.; Keshari, K. R. Multi-sample measurement of hyperpolarized pyruvate-to-lactate flux in melanoma cells. *NMR in Biomedicine* **2020**, *34*, e4447.

(16) Elliott, S. J.; Stern, Q.; Jannin, S. Solid-state ^{1}H spin polarimetry by [13]CH$_3$ nuclear magnetic resonance. *Magnetic Resonance* **2021**, *2*, 643–652.

(17) Koptyug, I. V.; Stern, Q.; Jannin, S.; Elliott, S. J. Frozen water NMR lineshape analysis enables absolute polarization quantification. *Physical Chemistry Chemical Physics* **2022**, *24*, 5956–5964.

(18) Ardenkjaer-Larsen, J. H.; Leach, A. M.; Clarke, N.; Urbahn, J.; Anderson, D.; Skloss, T. W. Dynamic nuclear polarization polarizer for sterile use intent. *NMR in Biomedicine* **2011**, *24*, 927–932.

(19) Kurhanewicz, J.; Vigneron, D. B.; Ardenkjaer-Larsen, J. H.; Bankson, J. A.; Brindle, K.; Cunningham, C. H.; Gallagher, F. A.; Keshari, K. R.; Kjaer, A.; Laustsen, C. et al. Hyperpolarized 13C MRI: Path to Clinical Translation in Oncology. *Neoplasia* **2019**, *21*, 1–16.

(20) Korchak, S. E.; Kilian, W.; Mitschang, L. Configuration and Performance of a Mobile[129]Xe Polarizer. *Applied Magnetic Resonance* **2012**, *44*, 65–80.

(21) Marco-Rius, I.; Tayler, M. C. D.; Kettunen, M. I.; Larkin, T. J.; Timm, K. N.; Serrao, E. M.; Rodrigues, T. B.; Pileio, G.; Ardenkjaer-Larsen, J. H.; Levitt, M. H. et al.

Hyperpolarized singlet lifetimes of pyruvate in human blood and in the mouse. *NMR in Biomedicine* **2013**, *26*, 1696–1704.

(22) Marco-Rius, I. Preserving hyperpolarised nuclear spin order to study cancer metabolism. **2014**,

(23) Vuichoud, B.; Milani, J.; Chappuis, Q.; Bornet, A.; Bodenhausen, G.; Jannin, S. Measuring absolute spin polarization in dissolution-DNP by Spin PolarimetrY Magnetic Resonance (SPY-MR). *Journal of Magnetic Resonance* **2015**, *260*, 127–135.

(24) Eichhorn, T. R.; Parker, A. J.; Josten, F.; Müller, C.; Scheuer, J.; Steiner, J. M.; Gierse, M.; Handwerker, J.; Keim, M.; Lucas, S. et al. Hyperpolarized Solution-State NMR Spectroscopy with Optically Polarized Crystals. *Journal of the American Chemical Society* **2022**, *144*, 2511–2519.

(25) Savukov, I. M.; Romalis, M. V. NMR Detection with an Atomic Magnetometer. *Physical Review Letters* **2005**, *94*, 123001.

(26) Tayler, M. C. D.; Theis, T.; Sjolander, T. F.; Blanchard, J. W.; Kentner, A.; Pustelny, S.; Pines, A.; Budker, D. Invited Review Article: Instrumentation for nuclear magnetic resonance in zero and ultralow magnetic field. *Review of Scientific Instruments* **2017**, *88*, 091101.

(27) Yashchuk, V. V.; Granwehr, J.; Kimball, D. F.; Rochester, S. M.; Trabesinger, A. H.; Urban, J. T.; Budker, D.; Pines, A. Hyperpolarized Xenon Nuclear Spins Detected by Optical Atomic Magnetometry. *Physical Review Letters* **2004**, *93*, 160801.

(28) Ganssle, P. J.; Shin, H. D.; Seltzer, S. J.; Bajaj, V. S.; Ledbetter, M. P.; Budker, D.; Knappe, S.; Kitching, J.; Pines, A. Ultra-Low-Field NMR Relaxation and Diffusion Measurements Using an Optical Magnetometer. *Angewandte Chemie International Edition* **2014**, *53*, 9766–9770.

(29) Bodenstedt, S.; Moll, D.; Glöggler, S.; Mitchell, M. W.; Tayler, M. C. D. Decoupling of Spin Decoherence Paths near Zero Magnetic Field. *The Journal of Physical Chemistry Letters* **2021**, *13*, 98–104.

(30) Shah, V.; Knappe, S.; Schwindt, P. D. D.; Kitching, J. Subpicotesla atomic magnetometry with a microfabricated vapour cell. *Nature Photonics* **2007**, *1*, 649–652.

(31) Tayler, M. C. D.; Mouloudakis, K.; Zetter, R.; Hunter, D.; Lucivero, V. G.; Bodenstedt, S.; Parkkonen, L.; Mitchell, M. W. Miniature Biplanar Coils for Alkali-Metal-Vapor Magnetometry. *Physical Review Applied* **2022**, *18*, 014036.

(32) Bodenstedt, S.; Mitchell, M. W.; Tayler, M. C. D. Fast-field-cycling ultralow-field nuclear magnetic relaxation dispersion. *Nature Communications* **2021**, *12*, 4041.

(33) Eichhorn, T. R.; Takado, Y.; Salameh, N.; Capozzi, A.; Cheng, T.; Hyacinthe, J.-N.; Mishkovsky, M.; Roussel, C.; Comment, A. Hyperpolarization without persistent radicals for in vivo real-time metabolic imaging. *Proceedings of the National Academy of Sciences* **2013**, *110*, 18064–18069.

(34) Pinon, A. C.; Capozzi, A.; Ardenkjær-Larsen, J. H. Hyperpolarized water through dissolution dynamic nuclear polarization with UV-generated radicals. *Communications Chemistry* **2020**, *3*.

(35) Gaunt, A. P.; Lewis, J. S.; Hesse, F.; Cheng, T.; Marco-Rius, I.; Brindle, K. M.; Comment, A. Labile Photo-Induced Free Radical in α-Ketoglutaric Acid: a Universal Endogenous Polarizing Agent for In–Vivo Hyperpolarized ^{13}C Magnetic Resonance. *Angewandte Chemie International Edition* **2021**, *61*, e202112982.

(36) Negroni, M.; Turhan, E.; Kress, T.; Ceillier, M.; Jannin, S.; Kurzbach, D. Frémy's Salt as a Low-Persistence Hyperpolarization Agent: Efficient Dynamic Nuclear Polarization Plus Rapid Radical Scavenging. *Journal of the American Chemical Society* **2022**, in press.

(37) Gajan, D.; Bornet, A.; Vuichoud, B.; Milani, J.; Melzi, R.; van Kalkeren, H. A.; Veyre, L.; Thieuleux, C.; Conley, M. P.; Grüning, W. R. et al. Hybrid polarizing solids for pure hyperpolarized liquids through dissolution dynamic nuclear polarization. *Proceedings of the National Academy of Sciences* **2014**, *111*, 14693–14697.

(38) Ji, X.; Bornet, A.; Vuichoud, B.; Milani, J.; Gajan, D.; Rossini, A. J.; Emsley, L.; Bodenhausen, G.; Jannin, S. Transportable hyperpolarized metabolites. *Nature Communications* **2017**, *8*, 13975.

(39) Capozzi, A.; Kilund, J.; Karlsson, M.; Patel, S.; Pinon, A. C.; Vibert, F.; Ouari, O.; Lerche, M. H.; Ardenkjær-Larsen, J. H. Metabolic contrast agents produced from transported solid 13C-glucose hyperpolarized via dynamic nuclear polarization. *Communications Chemistry* **2021**, *4*, 95.

(40) Capozzi, A. Design and performance of a small bath cryostat with NMR capability for transport of hyperpolarized samples. **2022**,

(41) Knecht, S.; Blanchard, J. W.; Barskiy, D.; Cavallari, E.; Dagys, L.; Dyke, E. V.; Tsukanov, M.; Bliemel, B.; Münnemann, K.; Aime, S. et al. Rapid hyperpolarization and purification of the metabolite fumarate in aqueous solution. *Proceedings of the National Academy of Sciences* **2021**, *118*, e2025383118.

(42) Marshall, A.; Salhov, A.; Gierse, M.; Müller, C.; Keim, M.; Lucas, S.; Parker, A.; Scheuer, J.; Vassiliou, C.; Neumann, P. et al. Radio-Frequency Sweeps at μT Fields for Parahydrogen-Induced Polarization of Biomolecules. 2022; https://arxiv.org/abs/2205.15709.

(43) Bastiaansen, J. A. M.; Merritt, M. E.; Comment, A. Measuring changes in substrate utilization in the myocardium in response to fasting using hyperpolarized [1-^{13}C]butyrate and [1-^{13}C]pyruvate. *Scientific Reports* **2016**, *6*, 25573.

(44) Qin, H.; Tang, S.; Riselli, A. M.; Bok, R. A.; Santos, R. D.; van Criekinge, M.; Gordon, J. W.; Aggarwal, R.; Chen, R.; Goddard, G. et al. Clinical translation of hyperpolarized ^{13}C pyruvate and urea MRI for simultaneous metabolic and perfusion imaging. *Magnetic Resonance in Medicine* **2021**, *87*, 138–149.

(45) QZFM Gen-2; QuSpin — quspin.com. https://quspin.com/products-qzfm/, [Accessed 10-Nov-2022].

(46) Twinleaf microSERF OPM. https://twinleaf.com/vector/microSERF/, Accessed 10-Nov-2022.

(47) Tierney, T. M.; Holmes, N.; Mellor, S.; López, J. D.; Roberts, G.; Hill, R. M.; Boto, E.; Leggett, J.; Shah, V.; Brookes, M. J. et al. Optically pumped magnetometers: From quantum origins to multi-channel magnetoencephalography. *NeuroImage* **2019**, *199*, 598–608.

(48) Brookes, M. J.; Leggett, J.; Rea, M.; Hill, R. M.; Holmes, N.; Boto, E.; Bowtell, R. Magnetoencephalography with optically pumped magnetometers (OPM-MEG): the next generation of functional neuroimaging. *Trends in Neurosciences* **2022**, *45*, 621–634.

(49) Savukov, I.; Kim, Y. J.; Schultz, G. Detection of ultra-low field NMR signal with a commercial QuSpin single-beam atomic magnetometer. *Journal of Magnetic Resonance* **2020**, *317*, 106780.

(50) Blanchard, J. W.; Wu, T.; Eills, J.; Hu, Y.; Budker, D. Zero- to ultralow-field nuclear magnetic resonance J-spectroscopy with commercial atomic magnetometers. *Journal of Magnetic Resonance* **2020**, *314*, 106723.

(51) Limes, M.; Foley, E.; Kornack, T.; Caliga, S.; McBride, S.; Braun, A.; Lee, W.; Lucivero, V.; Romalis, M. Portable Magnetometry for Detection of Biomagnetism in Ambient Environments. *Phys. Rev. Applied* **2020**, *14*, 011002.

Real-time polarimetry of hyperpolarized ^{13}C nuclear spins using an atomic magnetometer

Supporting Information

Kostas Mouloudakis[a], Marc Azagra[b], S Bodenstedt[a], Irene Marco-Rius[b], Morgan W. Mitchell[a,c], Michael C. D. Tayler[a,*]

[a]   *ICFO-Institut de Ciències Fotòniques, The Barcelona Institute of Science and Technology, 08860 Castelldefels (Barcelona), Spain.*

[b]   *IBEC – Institute for Bioengineering of Catalonia, 08028 Barcelona, Spain*

[c]   *ICREA – Institució Catalana de Recerca i Estudis Avançats, 08010 Barcelona, Spain.*

[*]   *Corresponding author. Email: michael.tayler@icfo.eu*

Contents

S.1 Experimental detail

The magnetic field of the nuclear-spin-polarized liquid sample was detected using the experimental setup illustrated in Figure S1 and Figure S2. Main parts of the setup are described in the following subsections.

S.1.1 Magnetic shielding

A commercial magnetic shield was used to passively screen background magnetic fields in the laboratory, up to several mT in magnitude, down to a residual of between 10 and 30 nT. The shield comprised three concentric outer layers of MuMetal and one innermost layer of ferrite (MS-1LF, Twinleaf LLC). The shield as receiver from the manufacturer also contained a set of XYZ printed-circuit coils on a flexible polyimide film attached to the interior of the ferrite layer, as shown in the Figure S1(b). These coils are normally intended to be used to supply compensatory magnetic fields along x-, y- and z-axes to achieve zero residual magnetic field inside the shield. In the present work, the x- and y-axis coils were used to supply the XY4 pulses (indicated in Figure 1 of the main manuscript) and the z-axis coil (Z) was unused. Field-to-current ratios were 69 nT/mA for the X coil and 130 nT/mA for the Y coil.

S.1.2 Atomic magnetometer

A linearly polarized 1 mW laser beam was generated by a vertical-cavity surface-emitting laser at the ^{87}Rb D$_1$ transition wavelength, around 795 nm. The beam was passed through a Keplerian telescope to adjust its width to around 3 mm and then a zero-order quarter-wave plate to generate circularly polarized light. The light then passed into the magnetic shield through the end hole and then through an optically dense alkali medium enclosed in a MEMS vapor cell. Cell external dimensions were 5 mm by 10 mm by 1.5 mm and internal path length 1 mm. The cell was locally heated to a temperature of around 150 °C using a resistive heater. The beam passing through the vapor was detected outside the magnetic shield, where it was focused on a low-noise amplified photodetector (Thorlabs model PDA36A2) and the resulting output voltage sampled using a 24-bit analog-to-digital converter integrated circuit at 48 ksps (Cirrus Logic CS4272) interfaced with a microcontroller (ARM Cortex M4F).

To operate the above apparatus as a magnetometer, the local magnetic field at the atomic vapor cell was modulated by applying a sinusoidal field along the z direction of 20 nT in amplitude and approximately 500 Hz in frequency. The field was supplied using a miniature biplanar printed-circuit coil set[1] positioned around the cell oven, as shown in Figure S1(b) in green. During modulation, the photodetector signal was sampled using the CS4272 and demodulated at the same frequency, then digital lowpass filtered to produce a quadrature signal whose amplitude was proportional to the dc bias field B_z. This field was the sum of the residual field inside the magnetic shield and the nuclear magnetic field of the hyperpolarized sample, seen at the position the atoms.

S2

S.1.3 Piercing solenoid

A 10-inch-long, 10-mm-o.d., 8.5-mm-i.d. flat-bottomed glass tube was used to contain the NMR sample during the magnetometry measurements. This was wrapped along its length with 0.15 mm diameter enameled copper wire to form a single layer solenoid coil, which when energized supplied a $30\,\mu$T bias field along the z axis; this field ensured that the spin polarization was always parallel to z, even when the sample was transported in and out of the magnetic shield. The bottom of the tube/solenoid structure sat atop the magnetometer oven as shown in Figure S1(b).

S.1.4 Pulsed field control

The alternating $(\pi)_x \equiv (\pi/2)_x(\pi)_y(\pi/2)_x$ and $(\pi)_y \equiv (\pi/2)_y(\pi)_{-x}(\pi/2)_y$ composite pulses constituting the XY4 pulse sequence shown in Figure 1 of the main paper were applied via bidirectional switching of direct current in the X and Y coils, as shown schematically in Figure S2. Current switching in both of the coils was performed using a dual-channel H-bridge circuit (Toshiba TB6612FNG on Pololu carrier board). The logic lines of the H-bridge circuit were controlled using the M4F microcontroller's digital input-output and were asynchronous with CS4272 data acquisition. The approximate duration of each π composite pulse was $50\,\mu$s on ^{1}H for a peak current of 0.5 A.

S.1.5 Additional notes

The table-top setup involving the magnetic shield, magnetometer and control electronics was constructed at ICFO and transported to IBEC in the rear passenger seat of a car belonging to one of the authors. The experiments described in the main manuscript were then performed at IBEC in the same laboratory as a commercial dissolution-DNP polarizer (HyperSense, Oxford Instruments Ltd.), as shown in Figure S1(a), on a vibrationally undamped table located approximately 1 m away from the polarizer magnet. The distance was chosen so that the magnetometer would be as close as possible to the polarizer without impeding access to its working parts.

References

[1] MCD Tayler, K Mouloudakis, R Zetter, D Hunter, VG Lucivero, S Bodenstedt, L Parkkonen and MW Mitchell, "Miniature biplanar coils for alkali-metal-vapor magnetometry", *Phys. Rev. Applied* **18**, 014036 (2022).

S3
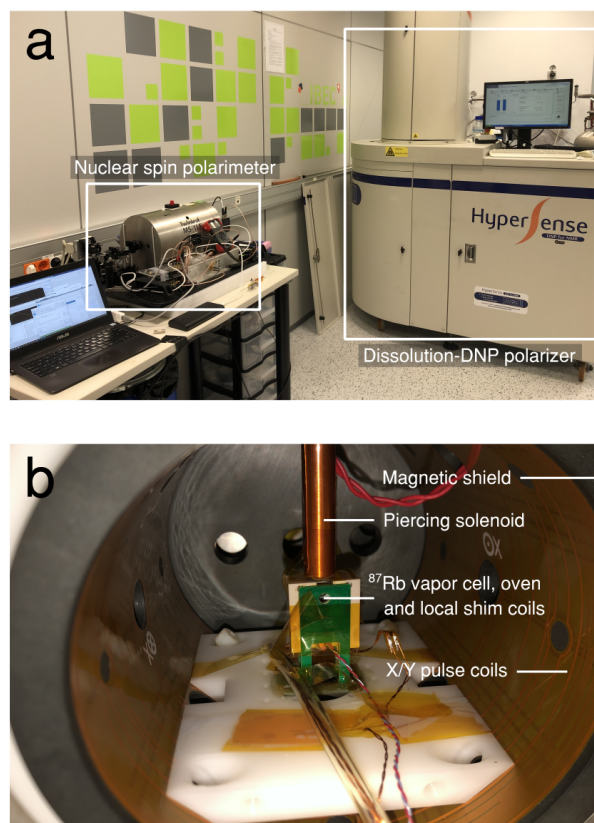
Fig. S1: Photographs of the experimental apparatus in use at the molecular-imaging-for-precision-medicine group at the Catalonia Institute for Bioengineering (IBEC): (a) the nuclear spin polarimeter, on top of a table approximately 1 m away from a commercial dissolution-DNP polarizer. The main visible feature of the setup is the cylindrical MuMetal magnetic shield; (b) a view of the interior of the magnetic shield, containing the coils for XY4 pulses on a flexible printed circuit board, the magnetometer, and a solenoid coil that surrounds the sample tube containing hyperpolarized liquid. A schematic version of (b) appears in the lower part of Figure S2 .

S4

23
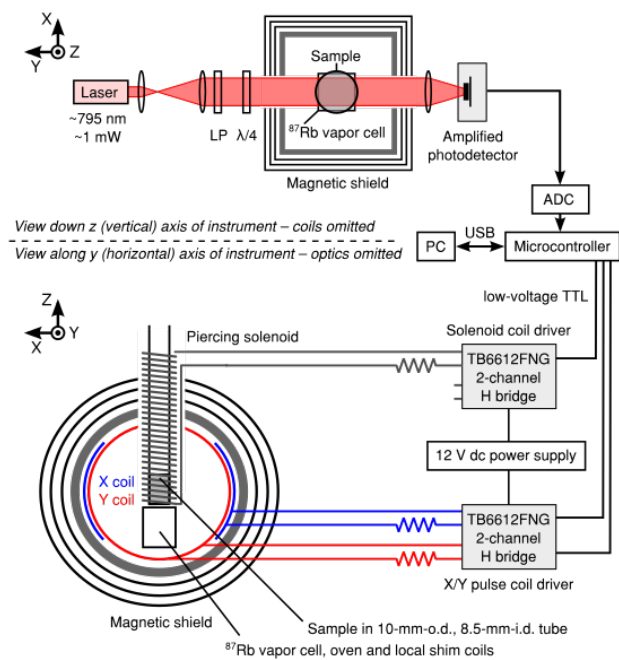
Fig. S2: Schematic view of the experimental setup for real-time nuclear spin polarimetry. The top half of the figure illustrates the magnetically shielded portion of the setup from a vertical point of view, down the z axis. The bottom half shows the view along the y axis, parallel to the laser beam.

S5

24